A novel Circular RNA circRBMS3 promote malignant tumor growth and metastasis through miR-424-eIF4B/YRDC axis

Zhe Gong
Zhejiang University School of Medicine Sir Run Run Shaw Hospital
Panyang Shen
Zhejiang University School of Medicine Sir Run Run Shaw Hospital
Haitao Wang
Zhejiang University School of Medicine Sir Run Run Shaw Hospital
Jinjin Zhu
Zhejiang University School of Medicine Sir Run Run Shaw Hospital
Shengyu Wang
Zhejiang University School of Medicine Sir Run Run Shaw Hospital
Kaiyu Liang
Zhejiang University School of Medicine Sir Run Run Shaw Hospital
Yining xu
Zhejiang University School of Medicine Sir Run Run Shaw Hospital
Shunwu Fan
Zhejiang University School of Medicine Sir Run Run Shaw Hospital
Shuying Shen
Zhejiang University School of Medicine Sir Run Run Shaw Hospital
Xiangqian Fang
Zhejiang University School of Medicine Sir Run Run Shaw Hospital
Gang Liu (11718332@zju.edu.cn)
Zhejiang University

Research

Keywords: CircRBMS3, tumorgenesis, miR-424, malignant tumor

Posted Date: September 21st, 2021

DOI: https://doi.org/10.21203/rs.3.rs-889437/v1

Abstract

Background

Circular RNAs (circRNAs) have been shown to have critical regulatory roles in tumorigenesis. However, the contribution of circRNAs to OS (osteosarcoma) remains largely unknown.

Methods

CircRNA deep sequencing was performed to the expression of circRNAs between OS and chondroma tissues. The regulatory and functional role of circRBMS3 (a circRNA derived from exons 7 to 10 of the *RBMS3* gene, hsa_circ_0064644) upregulation was examined in OS and was validated *in vitro* and *in vivo*, upstream regulator and downstream target of circRBMS3 were both explored. RNA pull down, a luciferase reporter assay, biotin-coupled microRNA capture and fluorescence *in situ* hybridization were used to evaluate the interaction between circRBMS3 and micro (mi)-R-424-5p. For *in vivo* tumorgenesis experiments, Subcutaneous and Orthotopic xenograft OS mouse models were built.

Results

Expression of circRBMS3 was higher in OS tissues due to the regulation of adenosine deaminase 1-acting on RNA (ADAR1), an abundant RNA editing enzyme. Our *in vitro* data indicated that ShcircRBMS3 inhibits the proliferation and migration of malignant tumor cells. Mechanistically, we show that circRBMS3 can regulate *eIF4B* and *YRDC*, through 'sponging' miR-424-5p. Furthermore, knockdown of circRBMS3 inhibited malignant phenotypes and bone destruction of OS *in vivo*.

Conclusions

Our results reveal an important role for a novel circRBMS3 in the growth and metastasis of malignant tumor cells and provide a fresh perspective on circRNAs in OS progression.

Introduction

Osteosarcoma (OS) mainly affects children and adolescents and is the most common primary malignant bone sarcoma [1]. In recent years, the prognosis of patients with OS has greatly improved owing to the combination of neoadjuvant chemotherapy, advanced diagnostic methods, and surgery [2]. Despite such progress, a large number of patients still respond poorly to normative drug therapy, as well as curative tumor resection, and suffer local relapse or distant metastasis [3]. Moreover, little is known concerning the underlying mechanisms surrounding oncogenesis, development, distant metastasis, and drug resistance in OS. Indeed, no precise diagnostic markers or effective therapeutic targets for OS have been discovered,

resulting in a diagnostic and treatment “bottleneck”. Therefore, it is of great importance to explore novel strategies to improve clinical outcomes.

Micro (mi)-RNAs are 19–25 nucleotides long, non-coding RNAs, that directly regulate target gene expression through binding to the 3'-untranslated region of target mRNAs. Increasing evidence suggests that aberrant expression of miRNA is frequent in a variety of tumors, and this expression exerts multiple influences in both promoting and/or inhibiting tumorigenesis, development and metastasis [4,5].

Competing endogenous RNAs (ceRNAs) are critical in determining gene expression regulation in many malignant tumors. Recent studies have found that dysregulation and disruption of ceRNA networks may play a predominant role in tumorigenicity [6]. Circular RNAs (CircRNAs), which are remarkably stable, show strong evolutionary conservation and high abundance, and have been shown to play crucial roles in the regulation of gene expression by mimicking ceRNAs. Intracellular circRNAs may act as miRNA ‘sponges’ that sequester miRNA by binding with MREs (microRNA response elements), leading to strong inhibition of miRNA activity, and therefore gene expression regulation [7]. Several studies have reported the role of circRNA as “miRNA sponges”, among which CDR1 as or ciRS-7 [8,9] appears to be the most understood. Containing 74 canonical binding sites for miR-7, CDR1as effectively combines with and sponges miR-7, leading to the attenuated interaction between CDR1 and miR7. CircRNA dysregulation has been found in various tumors, and a previous study indicated that certain circRNAs are aberrantly expressed in OS [10]. However, only preliminary studies on the role of circRNAs in OS have been performed [11,12,13], and the overall pathophysiological contributions of circRNAs to OS remain largely unknown.

In the present study, by using RNA-sequencing (RNA-seq), we compared the expression of circRNAs between OS and chondroma tissues. We further characterized one circRNA derived from exons 7–10 of *RBMS3* and termed it circRBMS3. The role of circRBMS3 in the growth and metastasis of tumors was further explored.

Materials And Methods

Cell culture and transfection

Human fetal osteoblasts hFOB1.19 was cultured in DMEM-F12 medium (Gibco) and Human osteosarcoma cell lines HOS and 143B were cultured in RPMI 1640 medium (Gibco) with 10% fetal bovine serum (FBS) (Gibco) and antibiotics (100 IU/mL penicillin and 100 lg/mL streptomycin). Cells were cultured according to standard techniques in a humidified incubator in 5% (v/v) CO2 atmosphere.

Analysis of circRNA expression profile

Our group obtained 12 osteoblastic osteosarcoma(IIB stage)and 12 chondroma tissues from patients at Department of Orthopaedic Surgery of the The Second Affiliated Hospital of Zhejiang University (Hangzhou, China) and Sir Run Run Shaw Hospital, Medical College of Zhejiang University (Hangzhou, China) with the permission from the Ethics Committee respectively, between 2016 and 2018 and

analyzed using the circRNAs chips. The microarray hybridization and collection of data were performed by KangChen Biotech, Shanghai, China. The five most up- and down-regulated circRNAs and their hierarchical clustering analysis were performed based on their expression value using the Cluster and TreeView program.

Sample separation by nLC and analysis by MS/MS.

After nephrectomy, fresh ccRCC and adjacent normal tissues were cut on ice to homogenize in 4 % SDS and 100m M Tris solution, following BCA assay for total protein concentration. Approximate 200 μg total protein from tissue was proteolysed on 10 kDa Filter (PALL Life Sciences) using a Filter Aided Sample Preparation (FASP) protocol. Tryptic digests for each sample were quantitated by colorimetric peptides assay. Peptide solution was then transferred to Solid Phase Extraction Cartridge (Empore 7mm/3ml) for desalting and clean-up of sample. Peptide samples were resuspended in water with 0.1% formic acid (v/v) and analyzed by nano-LC-MS/MS.

For label-free, relative quantitative analysis, 1 μg of the digest sample were analyzed by nano-LC-MS/MS, each sample were analysis once. LC separations were conducted on the Easy nano LC system (Thermo Scientific). Chromatography solvents were water (A) and acetonitrile (B), both with 0.1% formic acid. Peptide samples were concentrated and washed on an reverse phase trap column (75 μm × 2 cm; 5 μm; 100 Å; C-18, Thermo Scientific) with 0.1% formic acid, then they were eluted from the analytic column (75 μm × 50 cm; 3 μm; 100Å; C-18, Thermo Scientific) with the following gradient 5 to 40% B (130 min). At 140 min, the gradient increased to 90% B and was held there for 10 min. At 160 min, the gradient returned to 5% to re-equilibrate the column for the next injection. Eluting peptides were directly analyzed via tandem mass spectrometry (MS/MS) on an Fusion mass spectrometer (Thermo Scientific) equipped with a nanoelectrospray ion source. A spray voltage of 1.8 kV and an ion transfer tube temperature of 275°C were applied. The instrument was calibrated using standard compounds and operated in the data-dependent mode. The MS spectra were acquired in a data-dependent manner in the m/z range of 350 to 1800 and survey scans were acquired in Orbitrap mass analyzer at a mass resolution of 60,000 at 400 m/z. MS/MS data was acquired in the orbitrap at a mass resolution of 30,000 at 400 m/z using HCD (high collision dissociation) experiments, normalized collision energy of 30%, AGC for survey and MS/MS scans were 4e5 and 2e5 respectively. MS scans were recorded in profile mode, while the MS/MS was recorded in centroid mode, to reduce data file size. Dynamic exclusion was set to a repeat count of 1 with a 60 s duration.

Tissue culture

hFOB1.19, human OS, HOS, and 143B cell lines were purchased from FuHeng Cell Center (Shanghai, China). The OS cell lines were authenticated by the ShangHai Biowing Applied Biotechnology Co. Ltd., by STR profiling analysis, as described by Capes-Davis and according to the ANSI Standard (ASN-0002) set forth by the ATCC Standards Development Organization. Mycoplasma testing was performed using the Venor GeM Mycoplasma Detection Kit (Minerva Biolabs, Berlin, Germany). Detailed tissue culture

methods, as well as details of transfection and viral infection, can be found in the Supplementary information.

RNA extraction and quantitative real-time polymerase chain reaction (qRT-PCR)

TRIzol Reagent (Invitrogen) was used to extract total RNA from osteosarcoma tissues and cells. CircRNAs were amplified by divergent primer and RNase R was used to degrade linear RNA. QRT-PCR analysis on circular RNAs and mRNA was performed using Prime Script RT reagent Kit (TaKaRa) and SYBR Premix Ex Taq II (TaKaRa). β-actin was used as a control. For miR-424 analysis, miRNA was treated with DNase I to eliminate genomic DNA and cDNA was synthesized by Mir-X miR First-Strand Synthesis Kit (TaKaRa). SYBR Premix Ex Taq II (TaKaRa) was used for qRT-PCR. U6 was used as an internal standard control. Each sample was replicated three times and data was analyzed by comparing Ct values.

Cell proliferation assay and cloning formation assay

For cell proliferation assay, the transfected cells were seeded into 96-well plates at a density of 2000 cells per well. At 0, 24, 48, 72 and 96 h after seeding, cell viability was measured by the cell counting kit-8 (CCK-8) system (Dojindo, Japan) according to the manufacturer's instructions. Briefly, each well was added with 10 μl CCK-8 solution and the plate was incubated at 37°C for 1 h in dark. Absorbance at 450 nm of each well was measured using a microplate reader (Tecan, Switzerland).

For colony formation assay, 400 transfected osteosarcoma cells were seeded in 6-well plates. After 2 weeks of incubation, the cells were fixed with methanol and staining with 0.1% crystal violet and the colonies were imaged and counted.

Ago2-binding sites from CLIP data sets

The published online cross-linking immunoprecipitation (CLIP) data sets include Ago2 HITS-CLIP and PAR-CLIP data from several lymphoma cells and HEK-293 cells. We downloaded the available data sets from doRiNA (a database of RNA interactions in post-transcriptional regulation, http://dorina.mdc-berlin.de/regulators) and acquired the Ago2-binding sites of circRBMS3 genomic region.

Subcutaneous and Orthotopic xenograft OS mouse models

Nude mice (nu/nu, male 3- to 4-weeks-old) were injected subcutaneously or into the medullary cavity of tibia with 5×10^6 143B stable cells. Tumor volumes were calculated from the length (a) and width (b) by using the following formula: volume (ml^3) = $ab^2/2$. Five weeks after injection, the animals were sacrificed, and tumors were harvested, measured and weighed, and fixed in 4% paraformaldehyde. Wet tumor weight was calculated as mean weight ± standard deviation (SD) in each group.

MicroCT analysis

Tibias were scanned using high-resolution microcomputed tomography (Skyscan 1076) at 50 kV and 200 mA using a 0.5 mm aluminum filter. Images were captured every 0.6° through 180° rotation and analyzed using Skyscan software. Trabecular structures positioned 0.2 mm below the growth plate were quantified over a length of 1 mm. Bone volume (BV)/tumor volume (TV) and bone volume (BV) of cortical bones were determined.

RNA immunoprecipitation

The Ago-RIP assay was conducted in HOS cells using the Magna RIP RNA-Binding Protein Immunoprecipitation Kit (Millipore, Bedford, MA, USA). We first transfected the circRBMS3 siRNAs and sicontrol into HOS. Approximately 1×10^7 cells were sedimented and resuspended with an equal pellet volume of RIP Lysis Buffer plus a protease inhibitor cocktail and RNase inhibitors. Cell lysates (200 μl) were incubated with 5 μg of antibody against Ago2 (Millipore, Billerica, MA, USA) or control rabbit IgG-coated beads and mixed by rotation at 4°C overnight. After treating with proteinase K buffer, the immunoprecipitated RNAs were extracted by RNeasy MinElute Cleanup Kit (Qiagen, Duesseldorf, Germany) and reverse transcribed using Prime- Script RT Master Mix (TaKaRa, Tokyo, Japan). The abundance of circRBMS3 was detected by RT–qPCR assay.

Luciferase reporter assay

HEK293T cells were seeded in 96-well plates and cultured to 50–70% confluence before transfection. For circRBMS3 and miR-424, 600 ng plasmids of circRBMS3-wt and circRBMS3-mut, 20 nmol miR-424 and N.C. were transfected. After 48 h incubation, the Promega Dual-Luciferase system was used to detect firefly and Renilla luciferase activities. Using 100 ml Luciferase Assay Reagent II (LAR II) (Luciferase Assay Reagent, Promega) and, subsequently, 20 ml lysis buffer, firefly luciferase activities were measured to provide an internal reference, and Renilla luciferase activities were also measured using 100 ml Stop & Glo® Reagent (Luciferase Assay Reagent, Promega). Finally, the differences between firefly and Renilla luciferase activities were calculated to determine relative luciferase activity.

Cell apoptosis assays

To detect cell apoptosis, cells were stained using an annexin V-FITC/PI apoptosis kit (BD Biosciences, USA) and analyzed using flow cytometry. The ratio of early apoptotic cells and late apoptotic cells was compared to the values obtained for the controls in each experiment.

Western blot

Cells were lysed with radio immunoprecipitation assay buffer (RIPA, Beyotime, China), and protein was harvested and quantified by bicinchoninic acid (BCA) analysis (Beyotime, China). Protein extractions were separated by 10% SDS-PAGE and transferred onto polyvinylidene fluoride (PVDF) membranes (Sigma-Aldrich, USA). After the incubation with a high affinity anti-eIF4B antibody (1:1000) (abcam), anti-YRDC antibody (1:1000) (abcam) and anti-GAPDH antibody (1:2000) (Cell Signaling Technology, USA), the

membranes were then incubated with a secondary antibody (1:5000, Cell Signaling Technology, USA). After washes, signals were detected using a chemiluminescence system (Bio-Rad, USA) and analyzed using Image Lab Software.

Northern blot

Northern blot analysis was performed with northern blot kit (Ambion, USA). Briefly, about total RNAs (30 μg) of osteosarcoma cells were denatured in formaldehyde and then electrophoresed in a 1% agarose–formaldehyde gel. The RNAs were then transferred onto a Hybond-N + nylonmembrane (Beyotime, China) and hybridized with biotin-labeled DNA probes. Biotin chromogenic detection kit (Thermo Scientific, USA) was used to detect the bound RNAs. Finally, the membranes were exposed and analyzed using Image Lab software (Bio Rad, USA).

RNA *in situ* hybridization

Cy3-labeled locked nucleic acid miR-424 probes and Alexa Fluor 488-labeled circRBMS3 probes were designed and synthesized by RiboBio, using a Fluorescent *In Situ* Hybridization Kit (RiboBio) according to the manufacturer's instructions. Specimens were analyzed on a Nikon inverted fluorescence microscope.

Pull-down assay with biotinylated circRBMS3 probe

Briefly, 1×10^7 HOS and 143B cells were harvested, lysed, and sonicated. The circRBMS3 probe was incubated with C-1 magnetic beads (Life Technologies, Gaithersburg, MD,USA) at 25°C for 2 h to generate probe-coated beads. The cell lysates were incubated with circRBMS3 probe or oligo probe at 4°C overnight. After washing with wash buffer, RNA complexes were eluted and extracted for RT–qPCR or qPCR experiments. Biotinylated-circRBMS3 probe was designed and synthesized by RiboBio (Guangzhou, China).

Wound healing assay

HOS and 143B cells were cultured in six-well plates and scraped with the tip of a 200 μl pipette at timepoint 0. Cells migrating into 'wounded' areas were evaluated at 24 h using an inverted microscope (Olympus, Tokyo, Japan) and microphotographed. The healing rate was quantified by the extent of gap sizes.

Transwell migration and Matrigel ^{TM} invasion assays

Approximately 5×10^4 transfected cells were suspended in 200 μl of serum-free medium and seeded into the upper chambers of each transwell (8 μm pore size, Costar, NY, USA), which were coated with or without Matrigel (BD Biosciences, San Jose, CA, USA) for invasion and migration assays. The bottom chamber contained 10% FBS medium as a chemoattractant. The cells were incubated at 37°C with 5% CO_2 for the invasion assay (48 h) and for the migration assay (24 h). After incubation, cells in the top chamber were removed with cotton swabs and the cells on the lower surface were fixed and then stained

with 0.1% crystal violet. Migration and invasion rates were quantified by counting cells in at least 3 random fields.

Statistical analysis

Statistical analyses were performed with SPSS v22.0 software. Data are represented as means with SDs, and statistical significance was determined using unpaired Student's *t*-tests, unless indicated otherwise. *P* values less than 0.05 were considered statistically significant.

Results

CircRNA expression patterns in human OS and chondroma tissues

To generate a circRNA-profiling database, we performed circRNA deep sequencing of ribosomal RNA-depleted total RNA from clinical OS and chondroma tissues. RNA from three human osteoblastic osteosarcoma samples and three chondroma tissues were sequenced using an Illumina Hiseq X Ten. The reads obtained were mapped to reference ribosomal RNA (Bowtie2, http://bow tie-bio.sourceforge.net/bowtie2/) and to a reference genome (TopHat2, http://ccb.jhu.edu/software/tophat/) [14,15]. Twenty bases from either end of the unmapped reads were extracted and aligned to the reference genome, to identify unique anchor positions within the splice sites. Anchor reads that aligned in the reverse orientation (head-to-tail) indicated circRNA splicing and were then subjected to find_circ (https://omictools.com/find- circ-tool) to identify the circRNAs [16]. A candidate circRNA was identified if it was supported by at least two unique back-spliced reads in one sample. A total of 25224 circRNAs were identified using this approach (Supplementary Figure S1A) [17]. We next annotated the identified candidates using the RefSeq database [18]. Most of the circRNAs originated from protein-coding exons, while others aligned with introns, 5'-UTRs and 3'-UTRs (Supplementary Figure S1B). The majority of identified circRNAs were less than 2000 nucleotides (nt) in length (Supplementary Figure S1C). The chromosomal distribution of identified circRNAs showed no obvious differences between the OS and chondroma groups, while the total expression of circRNAs in the OS group was downregulated (Supplementary Figure S1D and E). Analysis of the number of circRNAs from host genes revealed that one gene could produce multiple circRNAs (Fig. 1F), which is consistent with previous reports[19]. We further investigated the abundance of circRNAs within one gene locus (n¼3,687). The thick line indicates the median, ends of the boxes define the 25th and 75th centiles and bars define the 5th and 95th centiles. The top five expressed circRNAs were presented in Supplementary Figure S1G. This result indicated that there is often a predominantly expressed circRNA isoform from one gene locus. The OS and chondroma groups displayed differential circRNA expression patterns (Fig. 1A). We focused on candidates that had the greatest differential expression between OS and chondroma groups, then matched them with circbase (http://www.circbase.org/. Among these specific candidates, novel_circ_0064644, which is formed by circularization of exon 7 to exon 10 of *RBMS3*, attracted our attention.

Identification Of Circrbms3 As A Circrna

To verify that exons 7 to 10 of *RBMS3* form an endogenous circRNA, we designed convergent and divergent primers that specifically amplified the canonical or back-spliced forms of *RBMS3* (Fig. 1B). Using cDNA and genomic DNA (gDNA) from HOS and 143B cell lines as templates, circRBMS3 could only be amplified using divergent primers, and no amplification product was observed from gDNA (Fig. 1B). By using reverse transcriptase-real-time polymerase chain reaction (RT-qPCR), we further confirmed that circRBMS3 was resistant to RNase R, while *RBMS3* mRNA levels were significantly reduced following RNase R treatment (Fig. 1C).

To investigate the function of circRBMS3 in OS development, we assayed the expression level of circRBMS3 in 12 pairs of chondroma and OS tissues, respectively, as well as in OS cell lines. Taking advantage of RT-qPCR and chromogenic *in situ* hybridization (CISH), we observed, consistent with the RNA-seq analysis, that circRBMS3 expression was higher in OS than in chondroma tissues or normal cells (Fig. 1D-F). Next, Sanger sequencing was used to confirm the circRBMS3 junction (Fig. 1G). Endogenous circRBMS3 was further revealed using a junction-specific probe in northern blotting (Fig. 1H). To establish the cellular localization of circRBMS3, we conducted fluorescence *in situ* hybridization (FISH) analysis. The junction probe detected abundant cytoplasmic circRBMS3 expression in HOS cells. Additionally, qPCR analysis from different cell fractions confirmed that circRBMS3 is predominantly located in the cytoplasm (Fig. 1I, lower panel).

The expression of circRBMS3 in OS can be regulated by ADAR1

It has been previously reported that *RBMS3* is a novel tumor suppressor gene, in esophageal squamous cell carcinoma (ESCC) [20], breast cancer [21], nasopharyngeal cancer (NPC) [22] and lung squamous cell carcinoma (LSCC)[23]. Although circRBMS3 was significantly upregulated in OS cell lines, the protein levels of RBMS3 were downregulated (Fig. 2I). This finding suggests that the higher expression of circRBMS3 in OS is not simply a by-product of splicing, but may be functional.

Next, we explored the reasons for circRBMS3 upregulation in OS, alongside RBMS3 mRNA and RBMS3 protein downregulation (Fig. 1J). As circRNAs could be regulated by RNA-binding proteins [24] post-transcriptionally, we assumed that circRBMS3, but not RBMS3 mRNA, is regulated by certain RNA-binding proteins post-transcriptionally during human OS development. To test this hypothesis, we measured the expression of circRBMS3 in OS cell lines after individually knocking down all two human RNA-binding proteins [25,26,27] reported to broadly regulate the biogenesis of circRNAs, including adenosine deaminase 1 acting on RNA (ADAR1) and DExH-Box Helicase 9 (DHX9). Among these two RNA-binding proteins, DHX9 has been reported to play an important role in OS devepment[28,29,30]. After knocking down ADAR1(p110), but not DHX9, circRBMS3 was upregulated, while RBMS3 mRNA did not show significant changes (Fig. 1K). Notably, mRNA and protein levels of ADAR1 were downregulated in OS cell lines (Fig. 1L). Taken together, the upregulation of circRBMS3 is, at least partly, caused by the downregulation of ADAR1 in human OS.

Effects of circRBMS3 on OS and other tumor cell lines

To further explore the biological functions of circRBMS3, we introduced two circRBMS3-knockdown short interfering (si)-RNAs, targeting the junction sites of circRBMS3 into HOS and 143B OS cells. The expression of circRBMS3 was significantly reduced in siRNA-transfected cells (Fig. 2A). Meanwhile, the expression of *RBMS3* mRNA showed no apparent change (Fig. 2B). To investigate the function of circRBMS3 in other tumor cells, we investigated the effect of circRBMS3 knockdown in sk-Hep1 (hepatic cellular carcinoma), AGS (gastric cancer), MCF-7 (breast cancer), HT1080 (sarcoma), and RBE (cholangiocarcinoma) cell lines (Supplementary Figure S2A). The proliferation and colony formation abilities of HOS and 143B cells decreased upon circRBMS3 inhibition (Fig. 2C-D), as did that of other tumor cell lines following circRBMS3 knockdown (Supplementary Figure S2B). Flow cytometric analysis was conducted to determine the effect of circRBMS3 knockdown on the apoptosis rate of OS cells and other tumor cells. Notably, inhibition of circRBMS3 augmented cellular apoptosis (Fig. 2E, Supplementary Figure S2C). Consistent with this, a wound-healing assay demonstrated a significant inhibition of cell migration in HOS and 143B cells following circRBMS3 knockdown (Fig. 2F). Moreover, inhibition of circRBMS3 also suppressed migration and invasion of OS cell lines and malignant tumor cell lines in transwell migration and Matrigel invasion assays (Fig. 2G, Supplementary Figure S2D). We also found that transfecting circRBMS3 siRNA did not affect the RBMS3 protein level (Fig. 2H). Knockdown of circRBMS3 did not alter total protein levels (Fig. 2I) or interaction of RBMS3 with its partners (Fig. 2J). Together, these results indicate that circRBMS3 is involved in tumor cell growth, migration, and invasion *in vitro*.

Molecular Mechanism Of Circrbms3 In Os

It has been previously reported that circRNA functions as an miRNA sponge in cancer cells[8,9]. As circRBMS3 is abundant in the cytoplasm, we performed an analysis using freely available AGO2 immunoprecipitation data, including high-throughput sequencing from doRiNA. We observed a high degree of AGO2 occupancy in the circRBMS3 region, which is highly conserved across several vertebrate species (Supplementary Figure S3A). To validate this result, we conducted RNA immunoprecipitation for AGO2 in 143B cells and found that endogenous circRBMS3 pulled-down from AGO2 antibodies was specifically enriched by RT-qPCR analysis when compared to circRBMS3 knockdown cells (Fig. 3A). To confirm whether circRBMS3 could aggregate miRNAs in OS cells, we selected 11 candidate miRNAs by overlapping the prediction results of miRNA recognition elements in the circRBMS3 sequence, using miRanda (Score Threshold > 140), Targetscan(at least 6mer binding site), and RNAhybrid (Fig. 3B). Next, we investigated whether circRBMS3 could directly bind these candidate miRNAs. A biotin-labeled circRBMS3 probe was designed and verified in OS cell lines, and the pull-down efficiency was established (Fig. 3C and D, Supplementary Figure S3B). The miRNAs were extracted following the pull-down assay, and the levels of 11 candidate miRNAs were determined by RT-qPCR. As shown in Fig. 4E, the miR-15a/497/424 cluster was the only one abundantly pulled down by circRBMS3 in both HOS and 143B cells. Because circRBMS3 contained miR-15a/497/424 binding sites (Fig. 3F), we transfected miR-

15a/497/424 mimics into HEK-293T cells and observed the insertion of the circRBMS3 binding sequence in the 3' untranslated region (3'-UTR) downregulated luciferase activity (Fig. 4G). Compared with controls, miR-424 decreased luciferase activity to the greatest extent, (~ 45%) (Fig. 3G). We then mutated the binding sites and transfection of the 3 miRNAs had no significant effect on luciferase activity when the corresponding target sites were mutated in the luciferase reporter (Fig. 3G). We then chose miR-424 for further investigation. FISH assays revealed that circRBMS3 interacts with miR-424 in the cytoplasm of OS cells (Fig. 3H). These results suggested that circRBMS3 functions as a sponge for miR-424.

MiR-424 inhibits OS cell migration, invasion, and proliferation in vitro

Using qPCR and FISH, we observed miR-424 downregulation in human OS samples compared with chondroma tissues (Fig. 4A and B). MiR-424 was also expressed at low levels in OS cells compared with hFOB1.19 cells (Fig. 4C). We then investigated whether miR-424 has a tumor repressor role during OS cell proliferation. Pre-miR-424 or miR-424 sponge were transfected into HOS and 143B cell lines, as well as the control vector. Expression of miR-424 was verified by RT-qPCR (supplementary Figure S3C & FigureS 4A). Results of CCK-8 and colony formation assays showed that overexpression of miR-424 in OS cells results in significant inhibition of cell proliferation (Fig. 4D and E, supplementary Figure S4B). In contrast, the proliferation rates of OS cells transfected with miR-424 sponge were significantly higher than those transfected with the control vector (Fig. 4D). Furthermore, we demonstrated that ectopic expression of miR-424 clearly increases the apoptosis rate 48 h after transfection of miR-424 mimics (Fig. 4F, supplementary Figure S4C). In addition, the wound healing assay (Fig. 4G) and Transwell assay (Fig. 4H, supplementary Figure S4D) showed that overexpression of miR-424 inhibits the migration and invasion of OS cells. Furthermore, Kaplan-Meier survival curves of the TCGA sarcoma dataset showed that patients with high expression (cut-off by the median gene expression value) of miR-424 had an elevated 10-year overall survival rate (Fig. 4I). These results confirmed that miR-424 reduced the proliferation, migration and invasion ability of osteosarcoma cells.

EIF4B **and** YRDC **are direct targets of miR-424**

Bioinformatics analysis was used to search for potential regulatory targets of miR-424. We got 1287 potential target of miR-424 from Targetscan (www.targetscan.org) with the standard "at least 6mer binding sites", 270 circRBMS3-regulating genes from RNA sequence and 190 circRBMS3-regulating proteins from Mass Spec analysis. We selected 5 candidate genes by overlapping the prediction results of gene recognition elements using mRNA sequencing, Targetscan, and Mass Spec analysis (Fig. 5A-D, Supplementary Figure S5A-H). Among these genes, EIF4B and YRDC, whose inhibition leads to the highest apoptosis rates in OS, were selected as targets for further analysis (Supplementary Figure S5I and J). RT-qPCR and immunohistochemistry demonstrated that EIF4B and YRDC were overexpressed in OS tissues compared with chondroma tissues (Fig. 5E-F). In addition, Kaplan-Meier survival curves from the TCGA sarcoma dataset showed that patients with high expression (cut-off by the median gene expression value) of EIF4B or YRDC had a lower 10-year overall survival rate (Fig. 5G).

To verify whether *EIF4B* and *YRDC* are direct targets of miR-424, we constructed 3'UTR sensors and co-transfected HEK-293T cells with miR-424 mimic or NC (negative control). We observed reduced luciferase activity of EIF4B and YRDC 3' UTR in the presence of miR-424 (Figs. 5H and I). To verify target specificity, we generated mutated forms of the *EIF4B* and *YRDC* 3'-UTR, in which the miR-424-binding site was abolished (Fig. 5H). Co-transfection of miR-424 mimics alongside the mutant construct abrogated the decrease in wild-type 3'-UTR luciferase activity, indicating that miR-424 specifically regulates EIF4B and YRDC expression (Fig. 5I).

To determine whether miR-424 could affect the expression of eIF4B and YRDC, HOS and 143B cells were transfected with miR-424 mimics, inhibitors, or respective controls. The results of immunofluorescence (Fig. 5J) and western blotting analyses (Fig. 5K) showed that miR-424 mimics markedly suppressed eIF4B and YRDC protein levels in OS cells, while the miR-424 inhibitor clearly promoted eIF4B and YRDC protein expression. Moreover, following transfection, mRNA and protein levels of eIF4B and YRDC were similarly downregulated (Fig. 5L). In summary, these results strongly suggest that miR-424 directly regulates eIF4B and YRDC in OS cell lines.

EIF4B and YRDC are known as oncogenes in some tumor types, while their function in OS is currently not understood. We explored the effect of eIF4B and YRDC on OS tumorigenesis by CCK-8 and colony formation experiments. There was a significant decrease in proliferation after inhibition of eIF4B and YRDC expression (*P < 0.05; Fig. 6A-B, supplementary Fig. 6A-C). Furthermore, knockdown of eIF4B and YRDC clearly induced higher levels of apoptosis (Fig. 6C, supplementary Fig. 6D, *P < 0.05). In addition, the wound healing (Fig. 6D) and transwell assays (Fig. 6E, supplementary Fig. 6E) showed that inhibition of eIF4B and YRDC inhibits the migration and invasion of tumor cells. These results suggested that eIF4B and YRDC are tumorigenic and are direct targets of miR-424.

Knockdown of miR-424 reverses shcircRBMS3-induced attenuation of OS cell proliferation, migration, and invasion

We co-transfected miR-424 sponge and the circRBMS3 knockdown construct into OS cells. Both protein and mRNA expression of eIF4B and YRDC significantly increased in OS cells co-transfected with shcircRBMS3 plasmid and the miR-424 sponge compared with cells transfected with shcircRBMS3 alone (Fig. 7A and B). Immunofluorescence analysis confirmed that the expression of eIF4B and YRDC increased in 143B and HOS cells transfected with shcircRBMS3 and miR-424 sponge together when compared with shcircRBMS3 alone (Fig. 7C). Knockdown of both miR-424 and circRBMS3 resulted in a higher growth rate than the circRBMS3 inhibition group (Fig. 7D). In addition, downregulation of both miR-424 and circRBMS3 promoted colony formation when compared with cells transfected with shcircRBMS3 alone (*P < 0.05 for both; Fig. 7E). Furthermore, apoptotic cell numbers were decreased after treatment with miR-424 sponge and shcircRBMS3 in co-transfected cells compared with shcircRBMS3 transfected cells. (Fig. 7F). Furthermore, wound healing assays (Fig. 7G) and transwell Matrigel ^{TM} invasion experiments (Fig. 7H) indicated that OS cells co-transfected with miR-424 sponge and shcircRBMS3 expression constructs demonstrated enhanced invasion and migration capabilities when

compared with shcircRBMS3-transfected cells. Strikingly, we observed that inhibition of miR-424 in OS cells significantly strengthened the anchorage-independent growth ability of circRBMS3 knockdown cells (Fig. 7I). Together, these data suggested that circRBMS3 promotes cell migration, invasion, and proliferation via sponging miR-424 and subsequently induces EIF4B and YRDC expression *in vitro*.

CircRBMS3 functions as miR-424 sponge to promote tumorigenesis in vivo

To explore the effects of circRBMS3 and miR-424 *in vivo*, 143B cells transfected with circRBMS3-deficient, miR-424 sponge, or vector were injected subcutaneously into nude mice for 35 days and then tumor volumes were measured. Compared with circRBMS3-deficient stable cell, cells lacking both miR-424 and circRBMS3 had a higher tumor growth rate (Fig. 8A and B). Similarly, co-expression of miR-424 inhibition and circRBMS3 knockdown constructs rescued the volume of 143B-derived tumors *in vivo* (Fig. 8C), compared with the circRBMS3-deficient group alone. We observed the same results for average tumor wet weight across all 3 groups (Fig. 8D).

To further evaluate the antitumor effect of circRBMS3 *in vivo*, an orthotopic OS model was established by intra-tibial injection of 143B cells. The mice were intra-tibial injected with circRBMS3-deficient, miR-424 sponge, or vector stable cells. As indicated in Fig. 8E and F, *in vivo* imaging results showed that circRBMS3 inhibited the growth of *in situ* tumors, while mice with tumors lacking both miR-424 and circRBMS3 had a higher tumor size and posterior limb weight (Figs. 8G).

We next evaluated the relationship between circRBMS3 and two target genes *in vivo*. CircRBMS3 knockdown reduced the levels of *eIF4B* and *YRDC* mRNA (Fig. 9H). This corresponded to a reduction of eIF4B and YRDC expression, as determined by western blot (Fig. 8K). Moreover, inhibition of both miR-424 and circRBMS3 rescued these effect (Fig. 8H-K). As shown in Fig. 8L, circRBMS3 knockdown in tumor tissues resulted in a significant increase of terminal dUTP nick end labeling (TUNEL)-positive cells, whereas the levels of Ki67, eIF4B or YRDC were decreased, while inhibition of miR-424 reversed these effects.

Furthermore, we investigated the effect of circRBMS3 on bone microarchitecture of the tumor-bearing tibia using micro computed tomography (CT) *in vivo*. As a result, circRBMS3 knockdown significantly reduced the bone destruction (Fig. 8M). Indeed, the trabecular bone volume (BV/TV; from 0.013 to 0.208) was significantly improved after circRBMS3 knockdown (Fig. 8M). The same tendency was observed for the BV (12.3 mm^3 in control vs. 21.3 mm^3 in treated group), while miR-424 inhibition rescued these effects (Fig. 8M). These results suggested that circRBMS3 acts as a sponge for miR-424, and that miR-424 mediates the tumorigenic function of circRBMS3 *in vivo* (Fig. 8N).

Discussion

In mammals, there is a novel class of stable and widely-endogenous RNAs that regulate gene expression, termed circular RNA (circRNAs) [31]. CircRNAs are more stable than linear RNA and are resistant to RNA exonuclease or RNase, due to their covalently-closed loop structures [32]. It has been suggested that

circRNAs may have important roles in malignant tumors, including gastric cancer, lung cancer, hepatocellular carcinoma, colon carcinoma, sarcoma and leukemia[33]. Due to the cell type and developmental stage-specific characteristics, circRNAs may also play roles in OS progression and provide new therapeutic targets for the treatment of OS.

Here, we screened circRNAs that are differentially expressed between OS and chondroma tissues by RNA-seq, focusing on the function and underlying mechanism of upregulated circRBMS3 expression in OS progression. RBMS3, which is also termed as the RNA binding motif, single stranded interacting protein 3, is a member of the MSSP family of proteins. RBMS3 is widely expressed from embryonic stages through to adulthood and can promote fibrosis of the liver and participate in the formation of cartilage. Recent studies have documented that RBMS3 is a novel tumor suppressor gene, including in breast cancer, esophageal squamous cell carcinoma, and nasopharyngeal carcinoma [20–23], thus attracting widespread attention. In particular, the level of RBMS3 in OS has not been investigated. Interestingly, in our study, the level of circRBMS3 was significantly upregulated in OS, while mRNA and protein levels of RBMS3 were downregulated. In addition, in vitro functional assays showed that knockdown of circRBMS3 could induce OS cell apoptosis, and inhibit OS cell proliferation, invasion, and migration. Based on post research, we confirmed that ADAR1 could downregulate the formation of circRBMS3 but have no effects on the mRNA.

We demonstrated the upstream signal of circRBMS3 and further investigate the downstream effectors of circRBMS3. In comparison to circRNAs, miRNAs are hugely well studied. Dysregulation of miRNA has been identified to be closely associated with tumorigenesis. Generally, miRNAs inhibit mRNA translation through binding to the 3'-UTR of target genes [34]. Previous studies have documented that miRNAs play important roles in OS progression and metastasis [35]. Notably, circRNAs mainly function as miRNA sponges, which results in a loss of miRNA function accompanied with increased levels of their endogenous targets [36]. CeRNA networks are complicated and the interactions between circRNAs and miRNAs have already been implicated as playing important roles in a variety of cancers. An important example is CDR1as a unique circRNA, for which more than 70 binding sites of miR-7 have been identified. CDR1as thus has an enormous capability to suppress miR-7 activity [16]. Another circRNA, termed circHIPK3, which is derived from exon 2 of HIPK3, was observed to serve as a sponge for miR-558 and miR-124 [37]. Here, we screened several predicted binding miRNAs via bioinformatics analysis, and confirmed that miR-424 was able to bind with circRBMS3 using a biotin-coupled probe pull down assay. MiR-424 is reported to be a tumor inhibitor in multiple cancers [38–40]. Our further functional studies and luciferase reporter assay also verified that miR-424 inhibits OS progression by directly targeting YRDC and eIF4B in OS.

Therefore, we present a novel regulatory axis formed by ADAR1-circRBMS3-miR-424-YRDC/eIF4B in OS. Taken together, we were able to confirm the regulatory role of circRBMS3 and its sponging effect on miRNAs in OS through functional and molecular analyses. The results were in full accordance with our hypothesis that circRBMS3 protects YRDC/eIF4B and promotes OS progression by sponging tumor

suppressive miRNAs. Besides, we also demonstrated that circRBMS3 is involved in other malignant tumor cell growth, migration, and invasion in vitro, such as breast cancer, gastric cancer, sarcoma, hepatic cellular carcinoma and cholangiocarcinoma cell lines. To our knowledge, this is the first report that generally investigates the expression, function, mechanism, and clinical implication of circRBMS3 in malignant tumors.

RNA binding protein has been reported to serve as a tumor suppressor gene that inhibits the development of various types of tumors, including glioblastoma, oral squamous cell carcinoma, gastric cancer, astrocytic glioma, and colon cancer [41–42]. RNA editing is a prominent post-transcriptional RNA process, generating RNA and protein diversity in eukaryotes. One common form of RNA editing is adenosine-to-inosine editing, which is dependent upon members of the family of adenosine deaminases that act on RNA (ADARs). In mammals, ADAR1 exists in many tissues, can edit non-coding RNAs, affects their biogenesis and alters their target gene specificity. ADAR1 has been demonstrated to affect various biological processes, including processing of miRNA [43], creating protein–protein complexes [44]and influencing gene expression [45]. ADAR1 has also been shown to be downregulated in melanoma development and ADAR1-editing miRNA-455-5p can inhibit melanoma growth and metastasis in vivo [46]. However, the role of ADAR1 in cancers remains unclear. The expression and function of ADAR1 in human OS has never been reported. In the current study, we found that mRNA and protein levels of ADAR1 were both significantly downregulated in OS cells, and that ADAR1 could inhibit the expression of circRBMS3, suggesting a tumor-suppressive role of ADAR1 in OS. However, ADAR1 obviously edit other circRNAs or lncRNAS in OS progression. Therefore, the function of ADAR1 requires further exploration. DHX9 is an abundant nuclear RNA helicase, mainly binds to inverted-repeat Alu elements. It can inhibit the production of circRNAs by binding to their flanking inverted complementary sequences and inhibiting the pairing of these sequences[28]. DHX9 has been reported to play an important role in OS devepment[28,29,30], however, in the current study, DHX9 knockdown did not affect the expression of circRBMS3 or RBMS3 mRNA.

Eukaryotic translation initiation factor 4B (eIF4B), which is necessary for ribosomal scanning through structured mRNA leaders [47,48], has been shown to be involved in the translation of numerous proliferative or anti-apoptotic mRNAs with highly structured 5' UTRs and subsequently affects cell growth and survival [49]. Abnormal phosphorylation or levels of eIF4B protein are closely linked with a variety of tumors including breast cancer, leukemia, Kaposi’s sarcoma, and lymphoma [50–52]. YRDC is ubiquitously expressed in human tissues, especially in the pancreas and liver. Recent studies have indicated that YRDC functions as an oncogene and can promote cell proliferation in bladder cancer, colon cancer, and gastric carcinoma [53–55]. However, little is known regarding the biology of these two genes in OS. To study the function of YRDC and eIF4B in OS, YRDC or eIF4B were knocked down using specific siRNAs. We found that either si-YRDC or si-eIF4B could lead to suppressive effects on OS cell proliferation and migration. Furthermore, luciferase reporter assay, immunofluorescence (IF), western blotting (WB), or RT-qPCR experiments were employed to further confirm that YRDC and EIF4B are direct targets of miR-424.

In conclusion, the current study investigated the regulatory function of a newly-found circRBMS3 (hsa_circ_0064644) that is upregulated in human OS, and which can efficiently sponge miR-424 to promote YRDC/eIF4B expression. Through the circRBMS3- miR-424-YRDC/eIF4B axis, circRBMS3 performed specific regulatory roles affecting the tumorgenesis of OS, as well as other malignant tumors. CircRBMS3 could be a novel biomarker of poor prognosis in OS. In addition, the circRBMS3- miR-424-YRDC/eIF4B axis is a novel signaling pathway, which could be a potential therapeutic target for OS patients. Our study also provides novel evidence to suggest that circRNAs act as “microRNA sponges” and may provide a new therapeutic target for the treatment of OS.

Conclsion

Our results reveal an important role for a novel circRBMS3 in the growth and metastasis of malignant tumor cells and provide a fresh perspective on circRNAs in OS progression. Mechanistically, *in vitro* and *in vivo* experiments in this study identified that CircRBMS3 acted as a ceRNA for miR-424 and regulated the EIF4B and YRDC expression in OS progression. Thus, the critical role of circRBMS3-miR-424-eIF4B/YRDC axis may appear to be a new diagnostic and therapeutic targets for OS.

Abbreviations

OS: Osteoarthritis; CircRNAs: Circular RNA; ADAR1:adenosine deaminase 1-acting; CeRNAs: Competing endogenous RNAs; MREs: MicroRNA response elements; RNA-seq: RNA-sequencing; qRT-PCR: Quantitative real-time polymerase chain reaction; RIP□RNA immunoprecipitation□FISH: Fluorescent In Situ Hybridization; CISH: Chromogenic in situ hybridization; ESCC: Esophageal squamous cell carcinoma; NPC: Nasopharyngeal cancer; LSCC: Lung squamous cell carcinoma; DHX9: DExH-Box Helicase 9; EIF4B: eukaryotic translation initiation factor 4B; YRDC: N6-threonylcarbamoyltransferase domain containing

Declarations

Ethical Approval and Consent to participate

The present study was approved by the Ethics Committee of Sir Run Run Shaw Hospital.

Consent for publication

Obitained

Availability of supporting data

The datasets used and/or analyzed during the current study are available from the corresponding author on reasonable request.

Competing interests

The authors declare no conflict of interest.

Funding

The study was sponsored by National Natural Science Foundation of China (81802680, 81871797, 81472064 and 81601925), Key Project of Zhejiang Medical Science and Technology Plan (2015145597), Key Project of Zhejiang Provincial Natural Science Foundation (LZ15H06002). Medical Science and Technology Project of Zhejiang Province (2017179447). No benefits in any form have been or will be received from a commercial party related directly or indirectly to the subject of this study.

Authors' contributions

Zhe Gong, Panyang Shen and Haitao Wang contributed equally to this work. Shunwu Fan , Shuying Shen, Xiangqian Fang and Gang Liu designed this study. Jinjin Zhu, Kaiyu Liang, Shengyu Wang, Yining Xu performed the experiments. Zhe Gong, Shuying Shen, Xiangqian Fang and Gang Liu wrote the manuscript. All authors analyzed the data and revised the manuscript. All authors read and approved the final manuscript.

Acknowledgments

Not applicable.

Authors' information

1.Department of Orthopaedic Surgery, Sir Run Run Shaw Hospital, Medical College of Zhejiang University & Key Laboratory of Musculoskeletal System Degeneration and Regeneration Translational Research of Zhejiang Province

Sir Run Run Shaw Institute of Clinical Medicine of Zhejiang University 3 East Qingchun Road, Hangzhou, Zhejiang Province, China, 310016

References

1. Lamoureux F, Trichet V, Chipoy C, Blanchard F, Gouin F, Redini F. Recent advances in the management of osteosarcoma and forthcoming therapeutic strategies. Expert Rev Anticancer Ther. 2007;7:169–81.
2. Liao D, Zhong L, Duan T, Zhang RH, Wang X, Wang G, et al. Aspirin Suppresses the Growth and Metastasis of Osteosarcoma through the NF-kappaB Pathway. Clin Cancer Res. 2015;21:5349–59.
3. Lamora A, Talbot J, Bougras G, Amiaud J, Leduc M, Chesneau J, et al. Overexpression of smad7 blocks primary tumor growth and lung metastasis development in osteosarcoma. Clin Cancer Res. 2014;20:5097–112.
4. Tay Y, Rinn J, Pandolfi PP. The multilayered complexity of ceRNA crosstalk and competition. Nature. 2014;505:344–52.

5. Wesselhoeft RA, Kowalski PS, Anderson DG. Engineering circular RNA for potent and stable translation in eukaryotic cells. Nat Commun. 2018;9:2629.
6. Yoshino H, Seki N, Itesako T, Chiyomaru T, Nakagawa M, Enokida H. Aberrant expression of microRNAs in bladder cancer. Nat Rev Urol. 2013;10:396–404.
7. Cottrell KA, Chaudhari HG, Cohen BA, Djuranovic S. PTRE-seq reveals mechanism and interactions of RNA binding proteins and miRNAs. Nat Commun. 2018;9:301.
8. Salzman J, Gawad C, Wang PL, Lacayo N, Brown PO. Circular RNAs are the predominant transcript isoform from hundreds of human genes in diverse cell types. PLoS One. 2012;7:e30733.
9. Hansen TB, Jensen TI, Clausen BH, Bramsen JB, Finsen B, Damgaard CK, et al. Natural RNA circles function as efficient microRNA sponges. Nature. 2013;495:384–8.
10. Liu W, Zhang J, Zou C, Xie X, Wang Y, Wang B, et al. Microarray Expression Profile and Functional Analysis of Circular RNAs in Osteosarcoma. Cell Physiol Biochem. 2017;43:969–85.
11. Xiao-Long M, Kun-Peng Z, Chun-Lin Z. Circular RNA. circ_HIPK3 is down-regulated and suppresses cell proliferation, migration and invasion in osteosarcoma. J Cancer. 2018;9:1856–62.
12. Liu X, Zhong Y, Li J, Shan A. Circular RNA circ-NT5C2 acts as an oncogene in osteosarcoma proliferation and metastasis through targeting miR-448. Oncotarget. 2017;8:114829–38.
13. Song YZ, Li JF. Circular RNA hsa_circ_0001564 regulates osteosarcoma proliferation and apoptosis by acting miRNA sponge. Biochem Biophys Res Commun. 2018;495:2369–75.
14. Langmead B, Salzberg SL. Fast gapped-read alignment with Bowtie 2. Nat Methods. 2012;9:357–9.
15. Kim D, Pertea G, Trapnell C, Pimentel H, Kelley R, Salzberg SL. TopHat2: accurate alignment of transcriptomes in the presence of insertions, deletions and gene fusions. Genome Biol. 2013;14:R36.
16. Memczak S, Jens M, Elefsinioti A, Torti F, Krueger J, Rybak A, et al. Circular RNAs are a large class of animal RNAs with regulatory potency. Nature. 2013;495:333–8.
17. Glazar P, Papavasileiou P, Rajewsky N. circBase: a database for circular RNAs. RNA. 2014;20:1666–70.
18. Pruitt KD, Tatusova T, Brown GR, Maglott DR. NCBI Reference Sequences (RefSeq): current status, new features and genome annotation policy. Nucleic Acids Res. 2012;40:D130-5.
19. Zhang XO, Wang HB, Zhang Y, Lu X, Chen LL, Yang L. Complementary sequence-mediated exon circularization. Cell. 2014;159:134–47.
20. Li Y, Chen L, Nie CJ, Zeng TT, Liu H, Mao X, et al. Downregulation of RBMS3 is associated with poor prognosis in esophageal squamous cell carcinoma. Cancer Res. 2011;71:6106–15.
21. Yang Y, Quan L, Ling Y. RBMS3 Inhibits the Proliferation and Metastasis of Breast Cancer Cells. Oncol Res. 2018;26:9–15.
22. Chen J, Fu L, Zhang LY, Kwong DL, Yan L, Guan XY. Tumor suppressor genes on frequently deleted chromosome 3p in nasopharyngeal carcinoma. Chin J Cancer. 2012;31:215–22.
23. Liang YN, Liu Y, Meng Q, Li X, Wang F, Yao G, et al. RBMS3 is a tumor suppressor gene that acts as a favorable prognostic marker in lung squamous cell carcinoma. Med Oncol. 2015;32:459.

24. Ashwal-Fluss R, Meyer M, Pamudurti NR, Ivanov A, Bartok O, Hanan M, et al. circRNA biogenesis competes with pre-mRNA splicing. Mol Cell. 2014;56:55–66.
25. Wang IX, So E, Devlin JL, Zhao Y, Wu M, Cheung VG. ADAR regulates RNA editing, transcript stability, and gene expression. Cell Rep. 2013;5:849–60.
26. Li ZZ, Kondo T, Murata T, Ebersole TA, Nishi T, Tada K, et al. Expression of Hqk encoding a KH RNA binding protein is altered in human glioma. Jpn J Cancer Res. 2002;93:167–77.
27. Bian Y, Wang L, Lu H, Yang G, Zhang Z, Fu H, et al. Downregulation of tumor suppressor QKI in gastric cancer and its implication in cancer prognosis. Biochem Biophys Res Commun. 2012;422:187–93.
28. Fidaleo M, Svetoni F, Volpe E, Miñana B, Caporossi D, Paronetto MP. Genotoxic stress inhibits Ewing sarcoma cell growth by modulating alternative pre-mRNA processing of the RNA helicase DHX9. Oncotarget. 2015;6:31740–57.
29. Cheng DD, Zhang HZ, Yuan JQ, Li SJ, Yang QC, Fan CY. Minichromosome maintenance protein 2 and 3 promote osteosarcoma progression via DHX9 and predict poor patient prognosis. Oncotarget. 2017;8:26380–93.
30. Zucchini C, Rocchi A, Manara MC, De Sanctis P, Capanni C, Bianchini M, et al. Apoptotic genes as potential markers of metastatic phenotype in human osteosarcoma cell lines. Int J Oncol. 2008;32:17–31.
31. Jeck WR, Sorrentino JA, Wang K, Slevin MK, Burd CE, Liu J, et al. Circular RNAs are abundant, conserved, and associated with ALU repeats. RNA. 2013;19:141–57.
32. Suzuki H, Tsukahara T. A view of pre-mRNA splicing from RNase R resistant RNAs. Int J Mol Sci. 2014;15:9331–42.
33. Meng S, Zhou H, Feng Z, Xu Z, Tang Y, Li P, et al. CircRNA: functions and properties of a novel potential biomarker for cancer. Mol Cancer. 2017;16:94.
34. Selbach M, Schwanhausser B, Thierfelder N, Fang Z, Khanin R, Rajewsky N. Widespread changes in protein synthesis induced by microRNAs. Nature. 2008;455:58–63.
35. Leichter AL, Sullivan MJ, Eccles MR, Chatterjee A. MicroRNA expression patterns and signalling pathways in the development and progression of childhood solid tumours. Mol Cancer. 2017;16:15.
36. Kristensen LS, Hansen TB, Veno MT, Kjems J. Circular RNAs in cancer: opportunities and challenges in the field. Oncogene. 2018;37:555–65.
37. Li Y, Zheng F, Xiao X, Xie F, Tao D, Huang C, et al. CircHIPK3 sponges miR-558 to suppress heparanase expression in bladder cancer cells. EMBO Rep. 2017;18:1646–59.
38. Hershkovitz-Rokah O, Modai S, Pasmanik-Chor M, Toren A, Shomron N, Raanani P, et al. Restoration of miR-424 suppresses BCR-ABL activity and sensitizes CML cells to imatinib treatment. Cancer Lett. 2015;360:245–56.
39. Yu L, Ding GF, He C, Sun L, Jiang Y, Zhu L. MicroRNA-424 is down-regulated in hepatocellular carcinoma and suppresses cell migration and invasion through c-Myb. PLoS One. 2014;9:e91661.

40. Yang H, Zheng W, Shuai X, Chang RM, Yu L, Fang F, et al. MicroRNA-424 inhibits Akt3/E2F3 axis and tumor growth in hepatocellular carcinoma. Oncotarget. 2015;6:27736–50.
41. Chen AJ, Paik JH, Zhang H, Shukla SA, Mortensen R, Hu J, et al. STAR RNA-binding protein Quaking suppresses cancer via stabilization of specific miRNA. Genes Dev. 2012;26:1459–72.
42. Fu X, Feng Y. QKI-5 suppresses cyclin D1 expression and proliferation of oral squamous cell carcinoma cells via MAPK signalling pathway. Int J Oral Maxillofac Surg. 2015;44:562–7.
43. Yang G, Fu H, Zhang J, Lu X, Yu F, Jin L, et al. RNA-binding protein quaking, a critical regulator of colon epithelial differentiation and a suppressor of colon cancer. Gastroenterology 2010;138:231 – 40 e1-5.
44. Heale BS, Eulalio A, Schulte L, Vogel J, O'Connell MA. Analysis of A to I editing of miRNA in macrophages exposed to Salmonella. RNA Biol. 2010;7:621–7.
45. Nemlich Y, Greenberg E, Ortenberg R, Besser MJ, Barshack I, Jacob-Hirsch J, et al. MicroRNA-mediated loss of ADAR1 in metastatic melanoma promotes tumor growth. J Clin Invest. 2013;123:2703–18.
46. Shoshan E, Mobley AK, Braeuer RR, Kamiya T, Huang L, Vasquez ME, et al. Reduced adenosine-to-inosine miR-455-5p editing promotes melanoma growth and metastasis. Nat Cell Biol. 2015;17:311–21.
47. Yang J, Wang J, Chen K, Guo G, Xi R, Rothman PB, et al. eIF4B phosphorylation by pim kinases plays a critical role in cellular transformation by Abl oncogenes. Cancer Res. 2013;73:4898–908.
48. Harms U, Andreou AZ, Gubaev A, Klostermeier D. eIF4B, eIF4G and RNA regulate eIF4A activity in translation initiation by modulating the eIF4A conformational cycle. Nucleic Acids Res. 2014;42:7911–22.
49. Sen ND, Zhou F, Harris MS, Ingolia NT, Hinnebusch AG. eIF4B stimulates translation of long mRNAs with structured 5' UTRs and low closed-loop potential but weak dependence on eIF4G. Proc Natl Acad Sci U S A. 2016;113:10464–72.
50. Madden JM, Mueller KL, Bollig-Fischer A, Stemmer P, Mattingly RR, Boerner JL. Abrogating phosphorylation of eIF4B is required for EGFR and mTOR inhibitor synergy in triple-negative breast cancer. Breast Cancer Res Treat. 2014;147:283–93.
51. Kuang E, Fu B, Liang Q, Myoung J, Zhu F. Phosphorylation of eukaryotic translation initiation factor 4B (EIF4B) by open reading frame 45/p90 ribosomal S6 kinase (ORF45/RSK) signaling axis facilitates protein translation during Kaposi sarcoma-associated herpesvirus (KSHV) lytic replication. J Biol Chem. 2011;286:41171–82.
52. Horvilleur E, Sbarrato T, Hill K, Spriggs RV, Screen M, Goodrem PJ, et al. A role for eukaryotic initiation factor 4B overexpression in the pathogenesis of diffuse large B-cell lymphoma. Leukemia. 2014;28:1092–102.
53. Huang B, Zhai W, Hu G, Huang C, Xie T, Zhang J, et al. MicroRNA-206 acts as a tumor suppressor in bladder cancer via targeting YRDC. Am J Transl Res. 2016;8:4705–15.

54. Tao G, Yang M, Jiang H, Yan Y, Wang X. The experiment on expression of human yrdC promotes proliferation of colon cancer SW-480 cells. Shanghai Med J. 2008;31:596–8.
55. Yang T, Shen X, Bi J, Huang S, Wei G, Zhu H, et al. Expression of human yrdC gene promotes proliferation of gastric carcinoma cells. The Chinese-German Journal of Clinical Oncology. 2009;8:433–7.

Figures

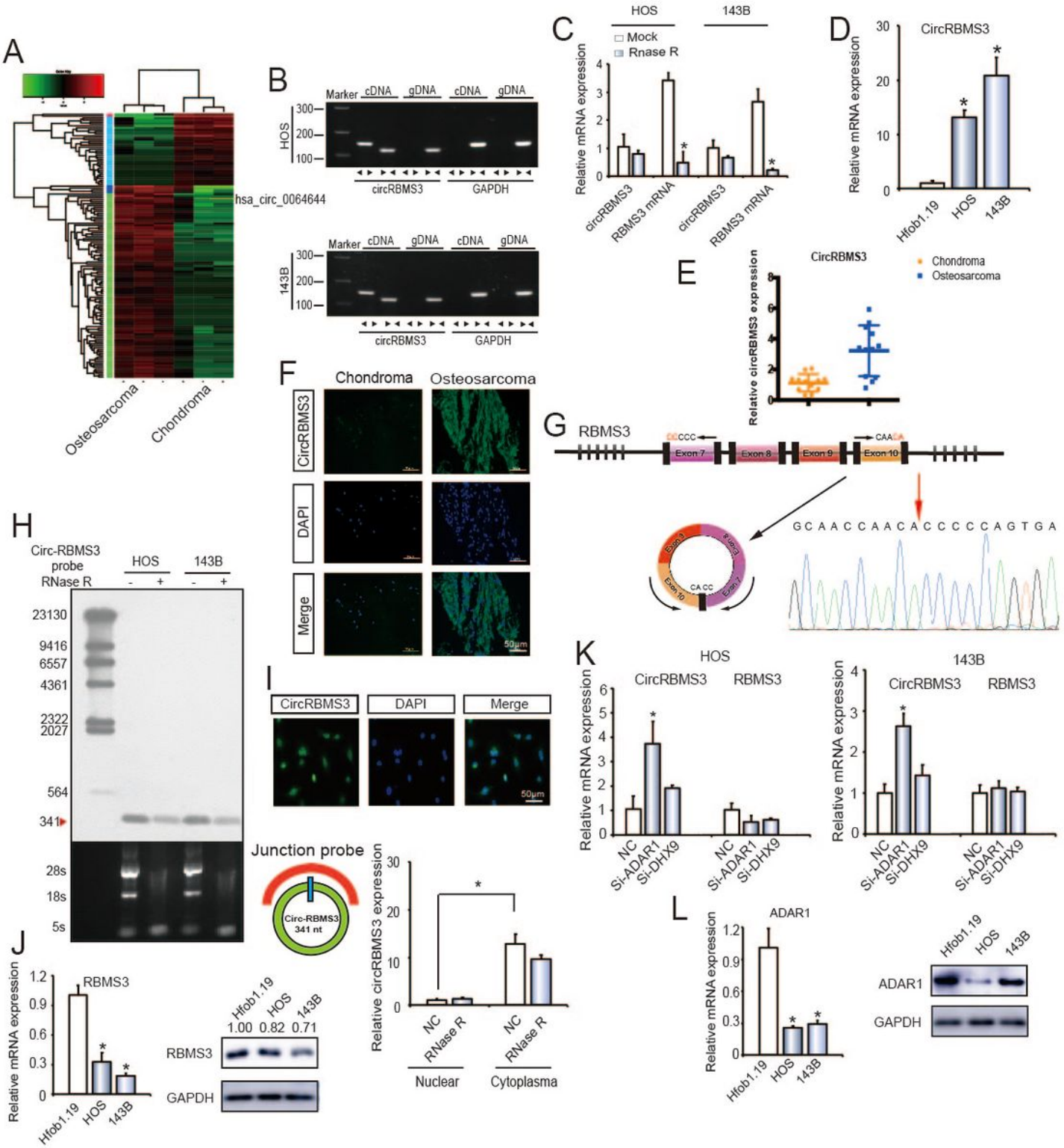

Figure 1

circRBMS3 validation and expression in OS tissue and cells. (A) Heat map of all differentially expressed circRNAs between chondroma and OS tumor tissues. (B) The presence of circRBMS3 was validated in HOS and 143B OS cell lines by RT–qPCR. Divergent primers amplified circRBMS3 in cDNA, but not in genomic DNA. GAPDH was used as a negative control. (C) The expression of circRBMS3 and RBMS3 mRNA in HOS and 143B cells treated with or without RNase R was detected by qPCR. The relative levels

of circRBMS3 and RBMS3 mRNA were normalized to the value measured in the mock treatment. Data represent the mean ± SD (n = 3). * P < 0.05. (D) CircRBMS3 expression in hFOB1.19 and OS (OS) cell lines (HOS and 143B) was evaluated by RT-qPCR. Data represent the mean ± standard deviation (SD) (n = 3). * P < 0.05 (E) CircRBMS3 expression was higher in human OS than in chondroma tissue. Data represent the mean ± SD (n = 12). (F) CircRBMS3 expression was higher in human OS than in chondroma tissue. Representative images are shown (400 × magnification). (G) Schematic illustration showing RBMS3 exon 7–10 circularization forming circRBMS3 (black arrow). The presence of circRBMS3 was validated by RT–qPCR, followed by Sanger sequencing. Red arrow represents “head-to-tail” circRBMS3 splicing sites. (H) Northern blots for detecting circRBMS3 in HOS and 143B cells treated with or without RNase R digestion. The upper panels show the probed blots of circRBMS3, and the red triangle represents the circRBMS3 band size (341 bp). The lower panels show the gel electrophoretic results of RNA with or without RNase R digestion. (I) RNA fluorescence in situ hybridization (FISH) showed that circRBMS3 was predominantly localized in the cytoplasm. CircRBMS3 probes were labeled with Alexa Fluor 488. Nuclei were stained with DAPI. Scale bar, 50 μm. Upper panel: FISH with junction-specific probes indicates the cellular localization of circRBMS3. Scale bars = 5 μM. Lower panel: circRBMS3 was detected in different cell fractions. Nuclear and cytoplasmic RNA was extracted, and junction primers were used for circRBMS3 detection. U6 was used as an internal control of nuclear RNA, and GAPDH was used as internal control for cytoplasmic RNA. Values are the average ± SD of 3 independent experiments. (J) RBMS3 expression in hFOB1.19 and OS (OS) cell lines (HOS and 143B) was evaluated by WB and RT-qPCR. Data represent the mean ± standard deviation (SD) (n = 3). * P < 0.05. (K) RT-qPCR for RBMS3 mRNA and circRBMS3 upon DHX9 and ADAR1 depletion using RNAi in OS cell lines. (L) ADAR1 expression in hFOB1.19 and OS cell lines (HOS and 143B) was evaluated by RT-qPCR and WB. Data represent the mean ± standard deviation (SD) (n = 3). * P < 0.05

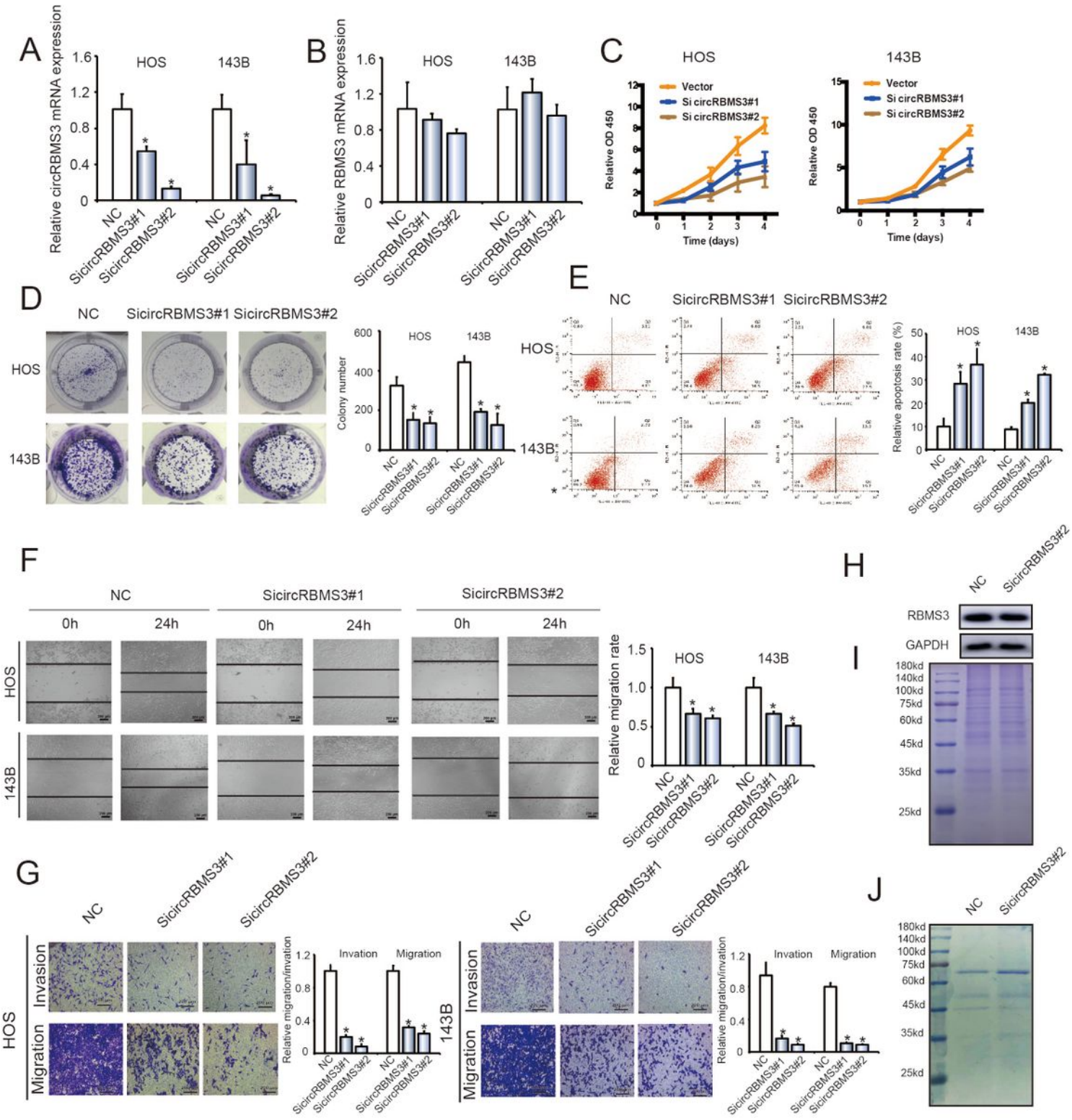

Figure 2

Knockdown of circRBMS3 inhibits the migration and invasion of OS cell lines in vitro. (A and B) The expression levels of circRBMS3 and RBMS3 mRNA in HOS and 143B cells after stable transfection of circRBMS3 short hairpin RNAs or vector plasmids were detected by qPCR. Data represent the mean ± SD (n = 3). *P < 0.05. (C) SiRNA-mediated circRBMS3 knockdown suppressed OS cell proliferation, as determined by CCK-8 assays. Data represent the mean ± SD (n = 6). (D) CircRBMS3 knockdown

suppresses cell growth, as determined by colony formation assays (details are shown in the insets). Error bars represent the mean ± SD of three independent experiments. * P < 0.05. (E) HOS and 143B cells were transfected with sicircRBMS3, followed by Annexin V-FITC/PI staining. The percentage of apoptotic cells is shown as the mean ± SD from three independent experiments. * P < 0.05, significantly different compared with the vector group. (F) The effect of sicircRBMS3 on cell migration capability was evaluated by wound healing assays using HOS and 143B cells. Data are the mean ± SD, n = 3. *P < 0.05. Scale bar, 200 μm. (G) CircRBMS3 knockdown suppresses cell migration and invasion abilities of HOS and 143B cells, as evaluated by transwell migration and MatrigelTM invasion assays. Data represent the mean ± SD (n = 3). * P < 0.05. Scale bar, 200 μm. (H) CircRBMS3 knockdown did not affect linear RBMS3 expression. (I) Total cell lysates were separated by SDS-PAGE and Coomassie blue staining. (J) Cell lysates were precipitated with anti-RBMS3 antibody followed by SDS-PAGE and Coomassie blue staining. Transfection with circRBMS3 siRNA did not affect the interaction of RBMS3 with its partners.

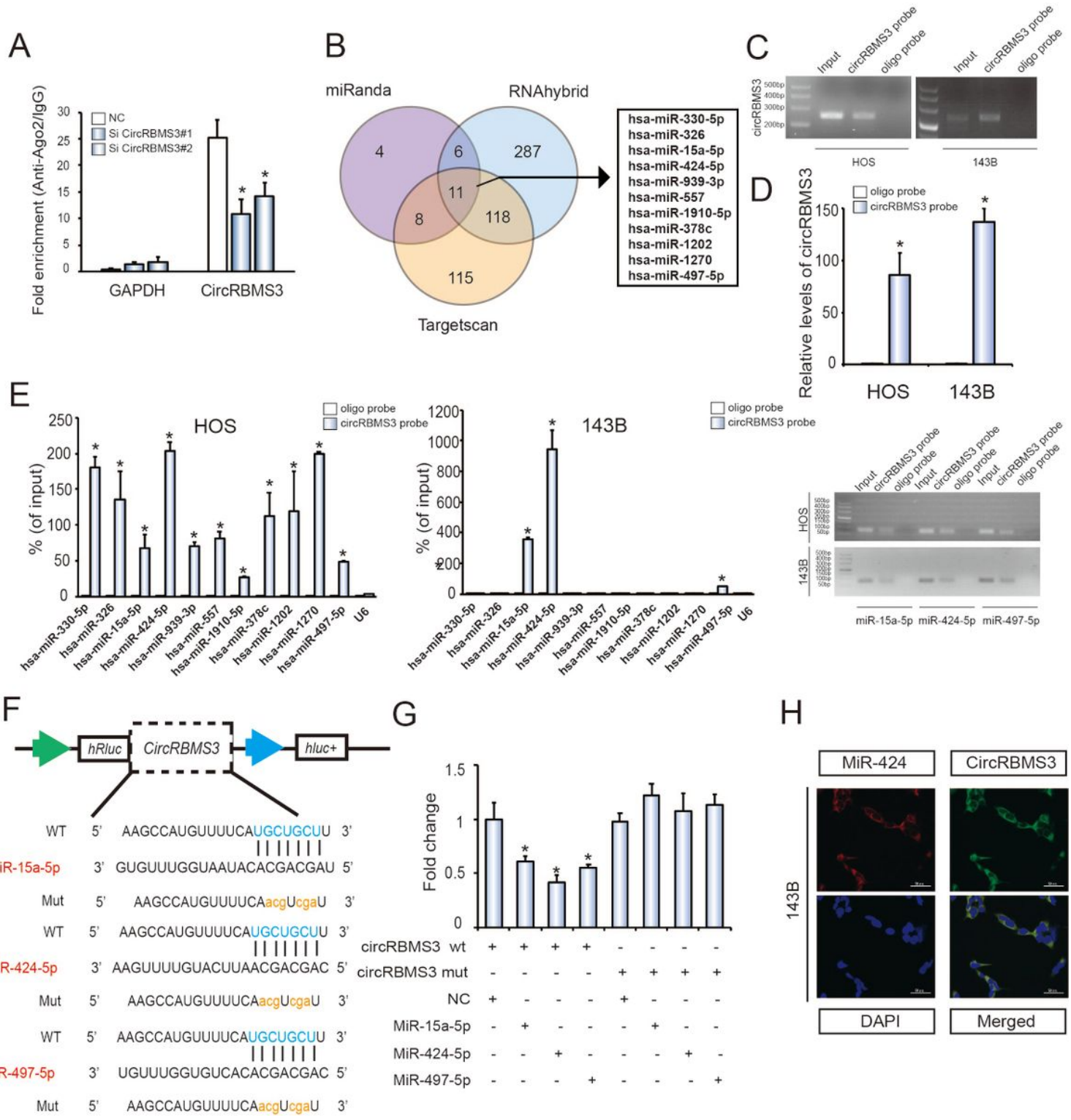

Figure 3

CircRBMS3 serves as a sponge for miR-424 in OS cells. (A) AGO2 RNA immunoprecipitation assay for circRBMS3 levels in 143B cells stably expressing shcircRBMS3. Data represent the mean ± SD for three experiments. * P < 0.05. (B) Schematic illustration showing overlapping of the target miRNAs of circRBMS3 predicted by miRanda, Targetscan, and RNAhybrid. (C-D) Lysates prepared from HOS and 143B cells were subjected to an RNA pull-down assay and tested by (C) RT–qPCR and (D) qPCR. Relative

levels of circRBMS3 were normalized to input. Data represent the mean ± SD (n = 3). * P < 0.05 versus oligo probe (Student's t-test). (E) The relative levels of 11 miRNA candidates in HOS and 143B cell lysates, as detected by qPCR and RT–qPCR. (F) Schematic illustration demonstrating complementary miR seed sequence with circRBMS3. Lowercase letters indicate mutated nucleotides. (G) 293T cells were co-transfected with miR mimics and a luciferase reporter construct containing wild-type (WT) or mutated (MUT) circRBMS3. Data represent the mean ± SD (n = 3). * P < 0.05. (H) FISH images showing co-localization of circRBMS3 and miR-424 in 143B cells. CircRBMS3 probes were labeled with Alexa Fluor 488. Locked nucleic acid miR-424 probes were labeled with Cy3. Nuclei were stained with DAPI. Scale bar, 50 μm.

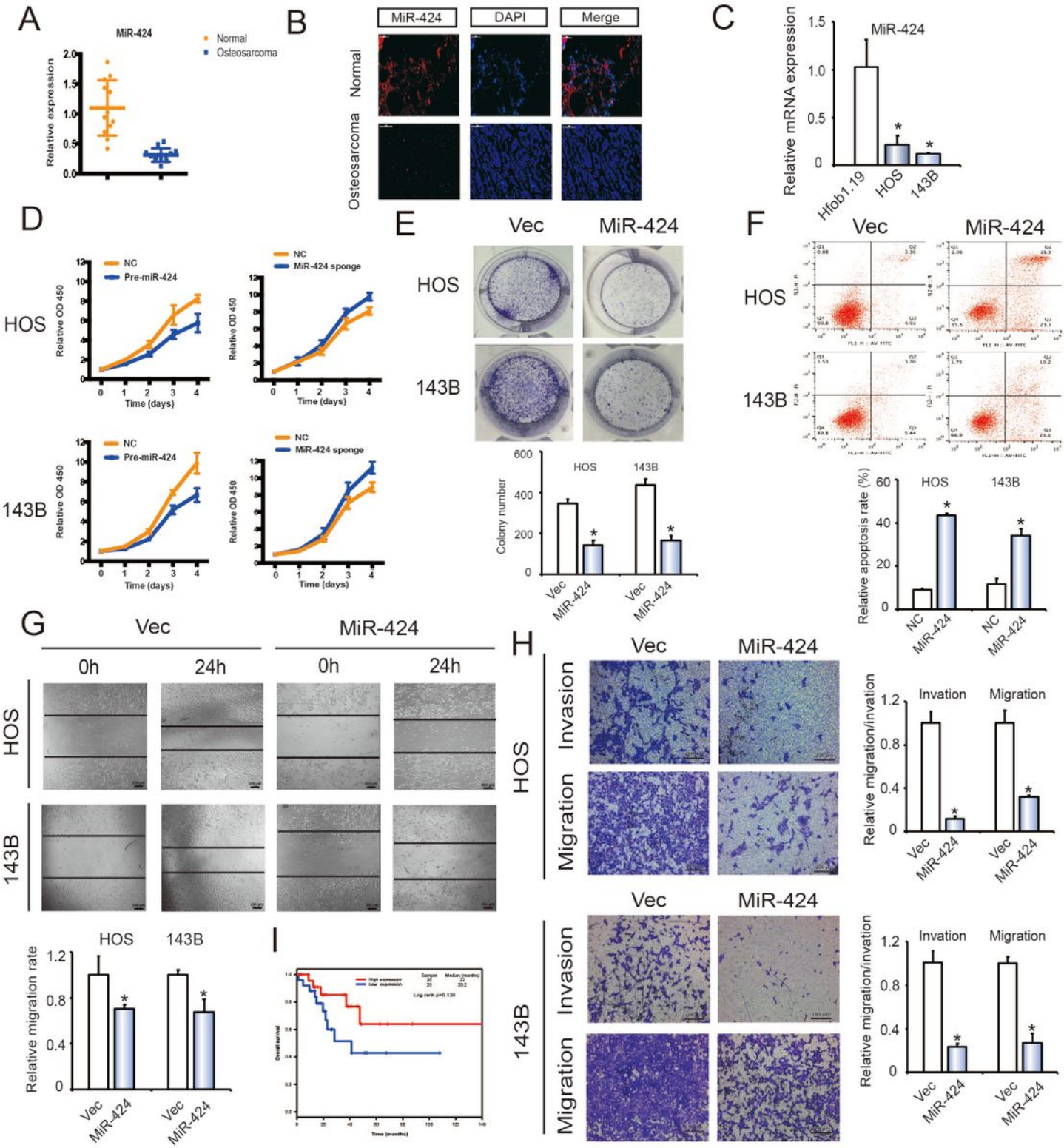

Figure 4

miR-424 is associated with OS cell migration and invasion (A) MiR-424 expression was lower in human OS than in chondroma tissue. Data represent the mean ± SD (n = 12). (B) MiR-424 expression was lower in human OS than in chondroma tissue. Representative images are shown. (C) MiR-424 expression in hFOB1.19 and OS cell lines (143B and HOS) was evaluated by RT-qPCR. Data represent the mean ± SD (n = 3). * P < 0.05. (D) MiR-424 overexpression did not affect circRBMS3 and RBMS3 expressions. (E) Pre-

miR-424 or miR-424 sponge mediated miR-424 overexpression and inhibition of OS cell proliferation, as determined by the CCK-8 assay. Data are presented as the mean ± SD (n = 6). (F) MiR-424 overexpression suppressed cell growth, as determined by the colony formation assay (details are shown in the insets). Error bars represent the mean ± SD of 3 independent experiments. * $P < 0.05$. (G) HOS and 143B cells were transfected with miR-424 mimics, followed by Annexin V-FITC/PI staining. The percentage of apoptotic cells is shown as the mean ± SD from 3 independent experiments. * $P < 0.05$, significantly different compared with the vector group. (H) The effect of pre-miR-424 on cell migration capability was evaluated by a wound-healing assay in HOS and 143B cells. Data are the mean ± SD, n = 3. * $P < 0.05$. Scale bar, 200 μm. (I) Cell migration and invasion of HOS and 143B cells, transfected with pre-miR-424 or vector, were evaluated by transwell migration and MatrigelTM invasion assays. Data represent mean ± SD (n = 3). * $P < 0.05$. Scale bar, 200 μm. (J) Kaplan-Meier survival analysis of miR-424 in OS patients (log rank test).

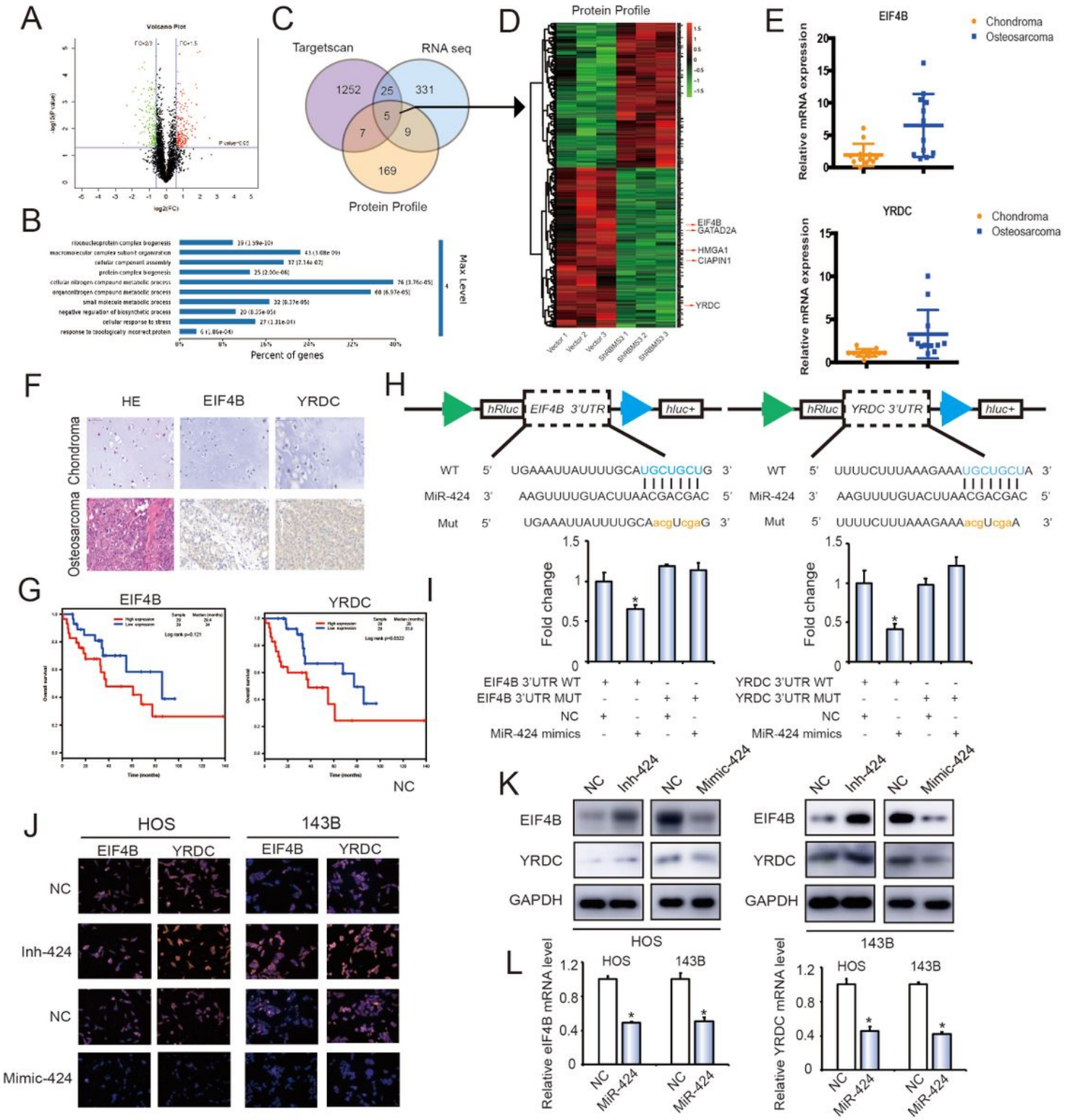

Figure 5

EIF4B and YRDC are direct targets of miR-424. (A) Volcano plots of protein profiles. 143B Cells were transfected with shcircRBMS3, followed by protein profiles, with 3 repeats for each sample. (B) KEGG analysis of protein profiles. 143B cells were transfected with shcircRBMS3, followed by protein profiles, with 3 repeats for each sample. (C) Schematic illustration showing overlapping of the target mRNAs of circRBMS3 and miR-424 predicted by RNA-seq, Targetscan, and by Mass Spec analysis. (D) Heatmap of

differentially expressed proteins after circRBMS3 knockdown. (E) EIF4B and YRDC expression levels were higher in human OS than in chondroma tissue examined by T test. Data represent the mean ± SD (n = 12). (F) EIF4B and YRDC expression levels were higher in human OS than in chondroma tissue. Representative images are shown. (G) Kaplan-Meier survival analysis of EIF4B and YRDC low and high sarcoma patients (log rank test). (H) Schematic illustration showing complementarity to the miR-424 seed sequence in the 3'-UTR of EIF4B and YRDC. Lowercase letters indicate mutated nucleotides. (I) 293T cells were co-transfected with pre-miR-424 and luciferase reporter constructs containing wild-type (WT) or mutated EIF4B and YRDC 3'-UTRs. Data represent the mean ± SD (n = 3). * $P < 0.05$. (J-L) MiR-424 overexpression reduced EIF4B and YRDC (J, K) protein and (L) mRNA levels while miR-424 inhibition increased EIF4B and YRDC (J, K) protein and (L) mRNA levels. Cells were transfected with NC or miR-424 mimic/inhibitor, and mRNA or protein levels evaluated. Protein expression was evaluated by western blot and immunofluorescence; mRNA levels were evaluated by RT-qPCR. Data represent the mean ± SD (n = 3). * $P < 0.05$. Scale bars = 50 μm.

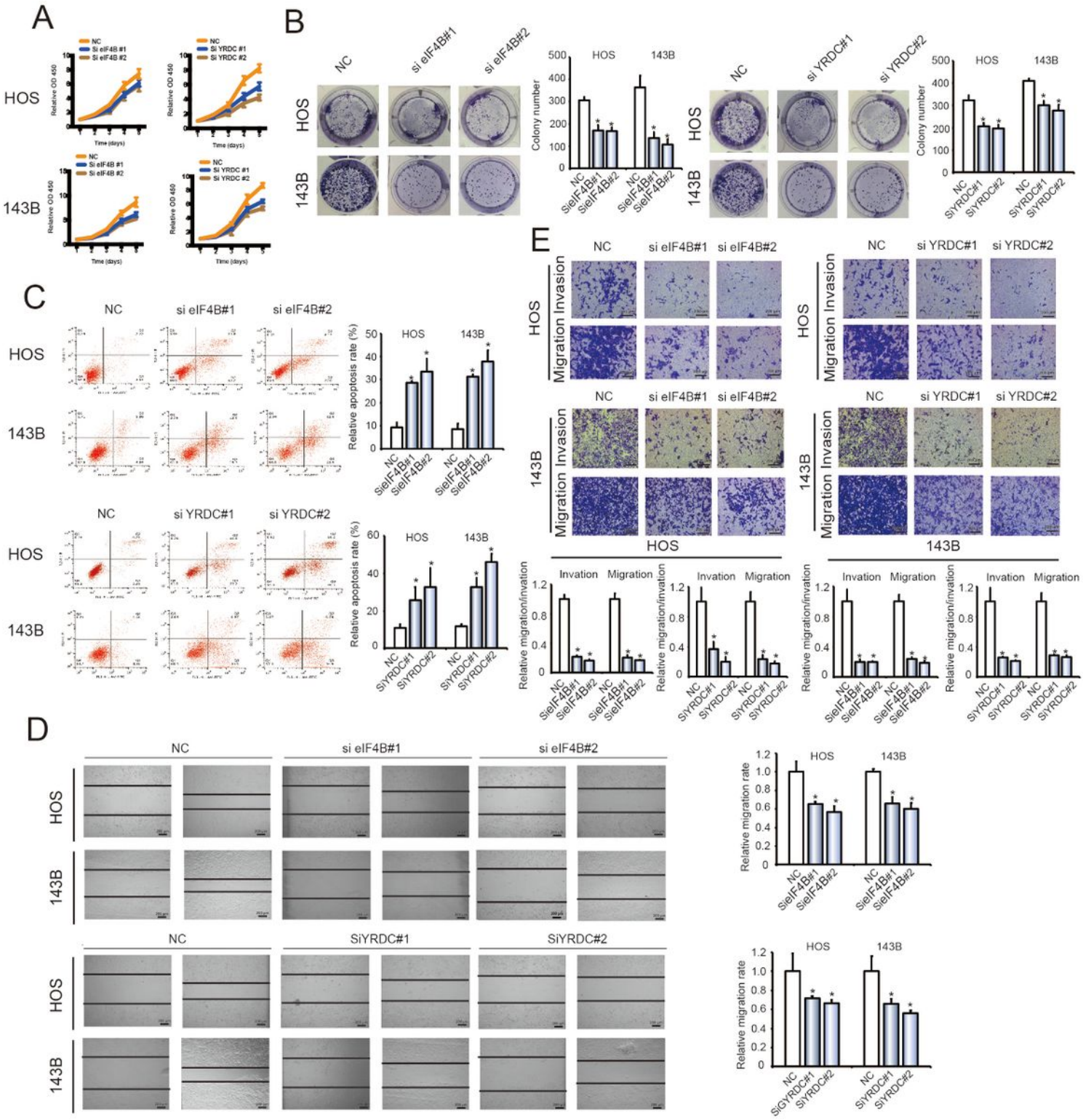

Figure 6

EIF4B and YRDC inhibit the migration and invasion of OS cells in vitro. (A) SiRNA-mediated EIF4B and YRDC knockdown suppressed OS cell proliferation, as determined in the CCK-8 assay. Data represent the mean ± SD (n = 6). (B) EIF4B and YRDC knockdown suppressed cell growth, as determined by the colony formation assay (details are shown in the insets). Error bars represent the mean ± SD of 3 independent experiments. * P < 0.05. (C) HOS and 143B cells were transfected with EIF4B or YRDC siRNA, followed by

Annexin V-FITC/PI staining. The percentage of apoptotic cells is shown as the mean ± SD from the 3 independent experiments. * P < 0.05, significantly different compared with the vector group. (D) The effect of EIF4B or YRDC siRNA on cell migration capability was evaluated by a wound-healing assay using HOS and 143B cells. Data are mean ± SD, n = 3. * P < 0.05. Scale bar, 200 μm. (E) EIF4B or YRDC knockdown suppresses cell migration and invasion abilities of HOS and 143B cells, as evaluated by Transwell migration and Matrigel invasion assays. Data represent the mean ± SD (n = 3). * P < 0.05. Scale bar, 200 μm.

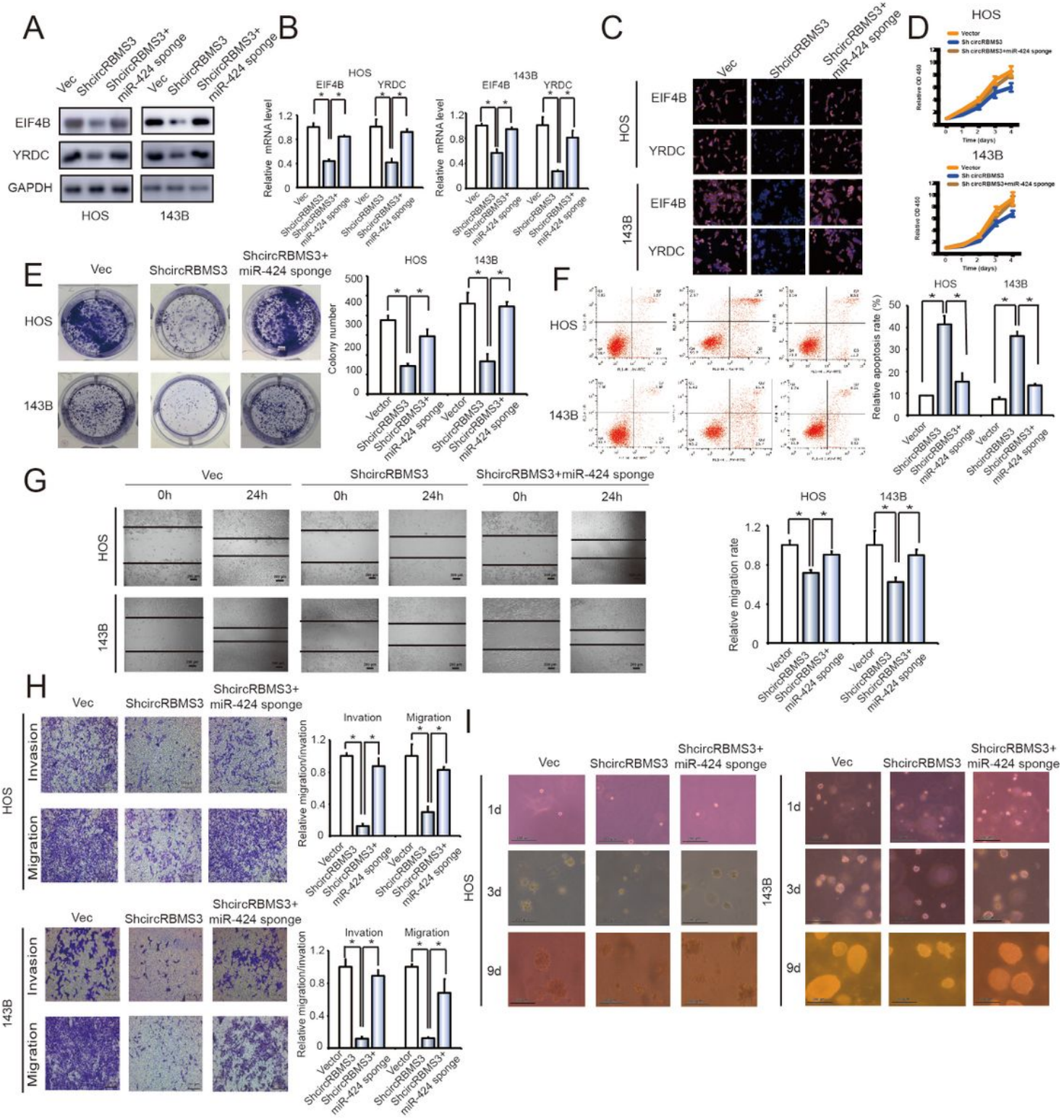

Figure 7

Knockdown of miR-424 reverses shcircRBMS3-induced attenuation of cell proliferation, migration, and invasion in OS cells. (A) The expression of EIF4B and YRDC in HOS and 143B cells was detected by western blot analysis. Cells were co-transfected with shcircRBMS3 and miR-424 sponge or control vector. Data represent the mean ± SD (n = 3). (B) The mRNA expression of EIF4B and YRDC in HOS and 143B cells was detected by RT-qPCR analysis. Cells were transfected with control vector and shcircRBMS3 with or without miR-424 sponge. Data represent the mean ± SD (n = 3). * $P < 0.05$ (C) The expression of EIF4B and YRDC in HOS and 143B cells was detected by immunofluorescence analysis. Cells were transfected with control vector and shcircRBMS3, with or without miR-424 sponge. Data represent the mean ± SD (n = 3). Scale bars = 50 μm. (D) Proliferation of OS cells transfected with control vector and shcircRBMS3, with or without miR-424 sponge, was evaluated by the CCK-8 assay. Data represent the mean ± SD of three independent experiments. (E) miR-424 downregulation rescued the growth inhibition of circRBMS3 knockdown in OS cells, as determined by colony formation assays (details are shown in the insets). Data represent the mean ± SD (n = 3). * $P < 0.05$. (F) Downregulation of both circRBMS3 and miR-424 resulted in fewer apoptotic cells in OS cells, compared with circRBMS3 inhibition alone. Apoptosis rates were determined by Annexin V-FITC/PI staining and FACS. Data represent the mean ± SD (n = 3). * $P < 0.05$. (G) The downregulation of circRBMS3 and miR-424 on cell migration capability was evaluated by a wound-healing assay in HOS and 143B cells. Data represent mean ± SD (n = 3). * $P < 0.05$. Scale bar, 200 μm. (H) Effects of circRBMS3 inhibition on cell migration and invasion were eliminated by miR-424 downregulation. Migration and invasion of OS cells transfected with control vector and shcircRBMS3, with or without miR-424 sponge, were evaluated by the MatrigelTM and transwell invasion assays. Scale bars = 50 μm. (I) OS cells transfected with control vector and shcircRBMS3 with or without miR-424 sponge were cultured in soft agar for 20 days. Colonies were photographed.

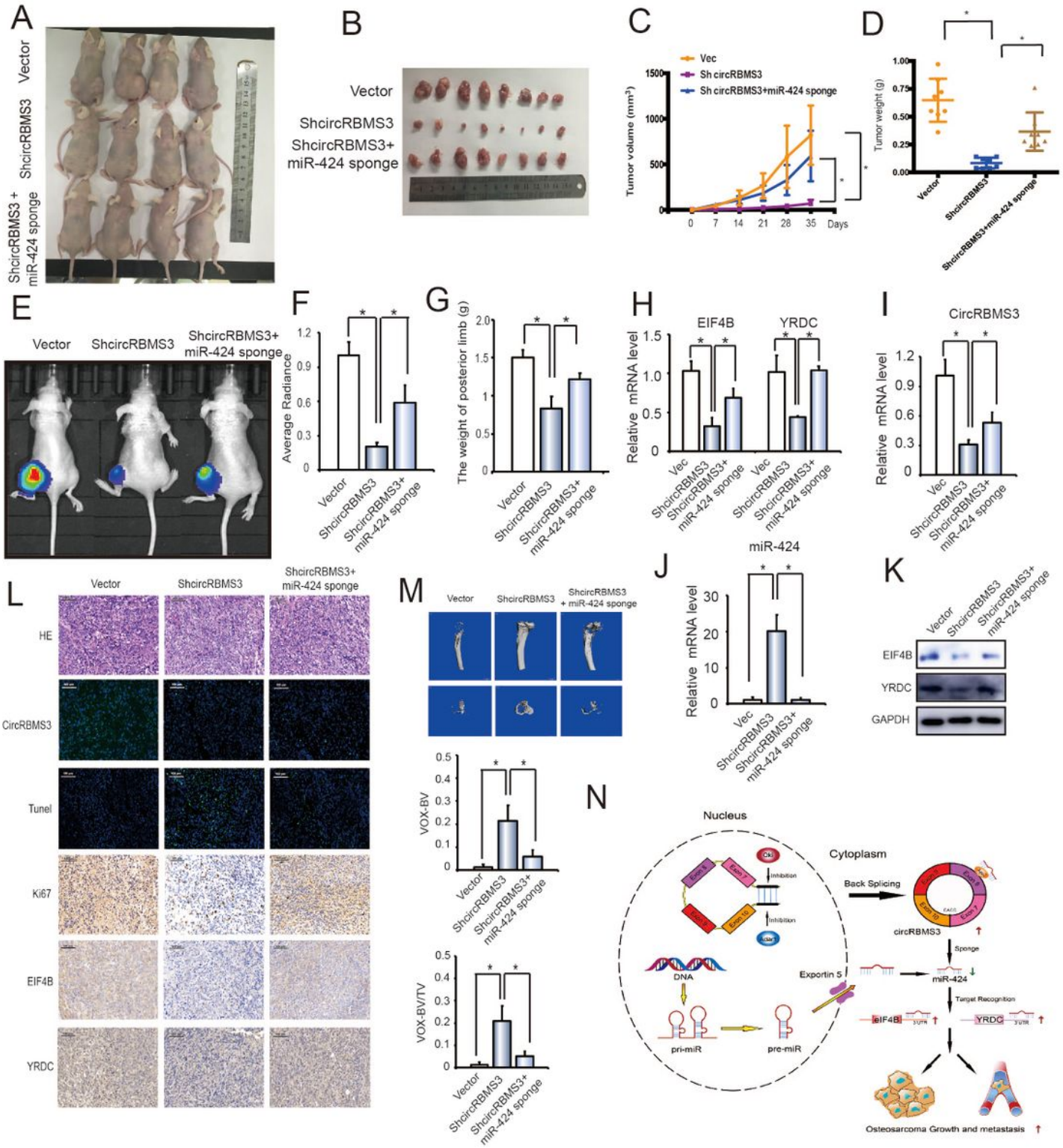

Figure 8

CircRBMS3 functions as a miR-424 sponge to promote tumorigenesis in vivo (A-B) Nude mice were injected with 5 × 106 143B stable cells. Four weeks later, tumors were dissected and photographed. (C) The graph represents tumor volumes (v = ab2/2) at injection with control cells or cells transfected with circRBMS3 short hairpin (sh)-RNA or co-transfected with circRBMS3 shRNA and miR-424 sponge (n = 6 per group). Data represent the mean ± SD (n = 8). (D) Average tumor weight in each group at the end of

the experiment. Data represent the mean ± SD (n = 8). * P < 0.05. (E) In vivo imaging of tibia tumor. (F) Average radiance of orthotopic xenograft nude mice. (G) The limb weight of orthotopic xenograft nude mice. (H) RT-qPCR analysis of EIF4B and YRDC expression in tumors from xenograft mice. (I and J) Knockdown efficiency of circRBMS3 and miR-424 in tumors from orthotopic xenograft nude mice. (K) Western blot analysis of EIF4B and YRDC in tumors from xenograft mice. (L) Histological analysis of tumor tissues by hematoxylin and eosin staining. EIF4B and YRDC expression was examined by immunohistochemistry. Representative images are shown. (M) MicroCT quantification of the specific trabecular bone volume [BV/TV (%)] and the cortical BV (mm3)] were calculated for the tibia of tumor-bearing mice in the different groups. (N) Schematic illustration of the circRBMS3/miR-424 axis.

Supplementary Files

This is a list of supplementary files associated with this preprint. Click to download.

- sup1.jpg
- sup2.jpg
- sup3.jpg
- sup4.jpg
- sup5.jpg
- SUP6.jpg